JOURNAL OF MATERIALS SCIENCE 15 (1980) 1387–1401

Stacking faults in chromium, iron and vanadium mixed carbides of the type M_7C_3

W. DUDZINSKI, J. P. MORNIROLI, M. GANTOIS
Laboratoire de génie métallurgique, Ecole des Mines, Parc de Saurupt, 54052 – Nancy–Cedex, France

Carbides found in white cast-iron containing 2.88% carbon, 15.22% chromium and 3.08% vanadium have the stoichiometric formula $Cr_{2.8}V_{0.7}Fe_{3.4}C_3$. They belong to the type M_7C_3 and are isomorphic with the chromium carbide Cr_7C_3. A modification of the approximate structure, given by Westgren, was considered in which carbon atoms were assumed to be situated right at the centre of gravity of perfectly symmetrical right-angled prisms. The great number of crystal defects that the carbides always contain were studied by electron microscopy and electron diffraction. They are stacking faults having as their fault planes one of the three equivalent planes $(1\,0\,\bar{1}\,0)$, $(1\,\bar{1}\,0\,0)$ or $(0\,1\,\bar{1}\,0)$, and as their fault vectors $\mathbf{R} = \mathbf{a}/2$ or $\mathbf{b}/2$ or $(\mathbf{a} + \mathbf{b})/2$. A detailed examination of the diffraction patterns which contain streaks or extra reflections indicates that, in strongly faulted carbides, the stacking faults are ordered. A simple model which views the structure of M_7C_3 as a stacking sequence of right-angled prisms containing carbon atoms is proposed. Using this model, the order of the stacking faults can be easily interpreted. It suggests that the stacking fault energy is very weak, hence the frequent occurrence of the stacking faults in the carbides.

1. Introduction

Chromium carbides of the type Cr_7C_3 found in steels, cast-irons or chromized surface layers, generally contain stacking faults. Several studies have been devoted to the chromium carbide Cr_7C_3 but they deal primarily with its crystallographic structure [1, 2], conditions of formation and transformation [3–5], and its relationship to Fe_3C [6], $Cr_{23}C_6$ [7] and other metal–transition carbides [8, 9].

The two studies of Dyson and Andrews [5] and Beech and Warrington [7] mention the presence of stacking faults in Cr_7C_3 and their effects on electron diffraction patterns. The purpose of the present study is to determine the main features of the stacking faults occurring in chromium carbides Cr_7C_3. To this end, a carbide isomorphic with Cr_7C_3 was chosen, namely a chromium–iron–vanadium mixed carbide present in a white cast-iron containing chromium and vanadium.

The samples were observed by electron microscopy and electron diffraction. Experimental results were analysed using a simple model which allows the nature, formation mechanism, frequency of appearance and order of stacking faults to be interpreted. An improvement in the mechanical properties of the alloys and of the surface layers in which the abrasion resistance of the M_7C_3 carbides is used is to be expected from a clearer understanding of these stacking faults.

2. Experimental procedures

Carbides were examined in white cast-iron samples of composition (wt %): 2.88% C, 15.22% Cr and 3.08% V. All the samples were taken from small ingots of an average weight of 2 kg which had not been subjected to any mechanical or thermal treatment after their solidification in a sand mould. Samples for electron microprobe analysis were in the form of small polished discs of a few mm thickness.

The carbides examined by X-ray diffraction were extracted from the matrix by anodic dissolution using a 5% hydrochloric acid, 95% distilled

0022–2461/80/061387–15$03.50/0

water solution as the electrolyte, with a d.c. potential of 9 V and a temperature of 20° C.

The thin foils used in transmission electron microscopy and electron diffraction were electropolished with a d.c. potential of 50 V in a 5% perchloric acid, 95% acetic acid solution, kept at a constant temperature of 14° C. The thin foils, which were finally ultrathinned for a few minutes by bombardment with argon ions, were observed using a PHILIPS EM 300 electron microscope equipped with a goniometer stage. The following experiments were performed with this instrument:

(1) trace analysis observing all the experimental procedures necessary to minimize the possible errors which may occur in this technique [10];

(2) image contrast experiments under two-beam kinematic conditions. The conditions which apply to the stacking fault studies were described in several papers by Gevers *et al.* [11] and by Whelan and Hirsch [12].

3. Experimental results

3.1. Morphology, composition and structure of the carbides

The structure of the cast-iron samples is dendritic. It is composed of a pearlitic matrix containing chromium, iron and vanadium mixed carbides. The extracted carbides appear in the form of faceted needles the shape of which is roughly that of a right-angled hexagonal prism (Fig. 1). Their composition, determined by electron microprobe analysis, is given in Table I. The atomic percentages lead to the formula $Cr_{2.8}V_{0.7}Fe_{3.4}C_3$ namely M_7C_3. Therefore, the carbide is stoichiometric with respect to carbon. This result is in accord with the works of Benz *et al.* [13], who showed that in the case of Cr_7C_3, elements such as iron, vanadium, molybdenium or magnesium can, to a greater or lesser extent, replace the chromium without modifying the stoichiometry with respect to carbon.

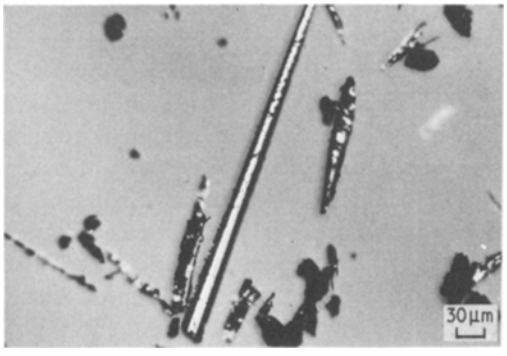

Figure 1 Optical micrograph showing carbides extracted by anodic dissolution. Their shape is roughly that of a hexagonal prism.

TABLE I Composition of carbides as determined by electron microprobe analysis on CAMECA MS46 and ARL SEMQ microprobes

	Chromium	Vanadium	Iron	Carbon
wt%	34.9	8.8	45.6	8.9
at%	28.0	7.1	33.9	30.9

The carbides can be derived, in view of their composition, by the substitution of either the chromium carbide Cr_7C_3 or of the iron carbide Fe_7C_3. All X-ray diffraction patterns of extracted carbides (Fig. 2) were indexed on the basis of a hexagonal unit cell with the parameters $a = 13.958$ Å and $c = 4.495$ Å. This cell corresponds to that proposed in 1935 by Westgren [1] to describe approximately Cr_7C_3. His cell (Fig. 3a), hexagonal in shape, has a trigonal symmetry and the lattice parameters have the values $a = 13.98$ Å and $c = 4.52$ Å. It belongs to the space group P31*c* and contains 56 chromium atoms and 24 carbon atoms whose co-ordinates are given in Table II. In this description, the z co-ordinates of the atoms are imprecise. It should be noted that a projection of the atoms onto the basal plane can be divided into four equal parts.

By analogy with Mn_7C_3 [14], Rouault *et al.* [2] proposed two other structures for Cr_7C_3: (i) a high-temperature structure referred to as the stable form, with an orthorhombic cell with lattice parameters $A = 7.010$ Å, $B = 12.142$ Å and $C = 4.52$ Å (Fig. 4c) and belonging to the space group *Pmcn*; (ii) a poorly crystallized structure, called the low-temperature form, observed in carbides prepared at temperatures lower than 1200° C. The cell is here hexagonal and has dimensions near to those of the ruthenium boride Ru_7B_3.

Aronsson [15] has shown that this boride, which he described with the aid of a hexagonal cell with the parameters $a_0 = 7.467$ Å and $c_0 = 4.713$ Å (Figs. 3a and 4a), has many structural similarities with the three carbides Cr_7C_3, Mn_7C_3 and Fe_7C_3. As a matter of fact, if one ignores the z co-ordinates, the arrangement of the ruthenium atoms in Ru_7B_3 corresponds almost exactly to that of the chromium atoms in one of the four parts of Westgren's hexagonal cell. Hence, in view of the lattice parameters of the two structures, one can consider

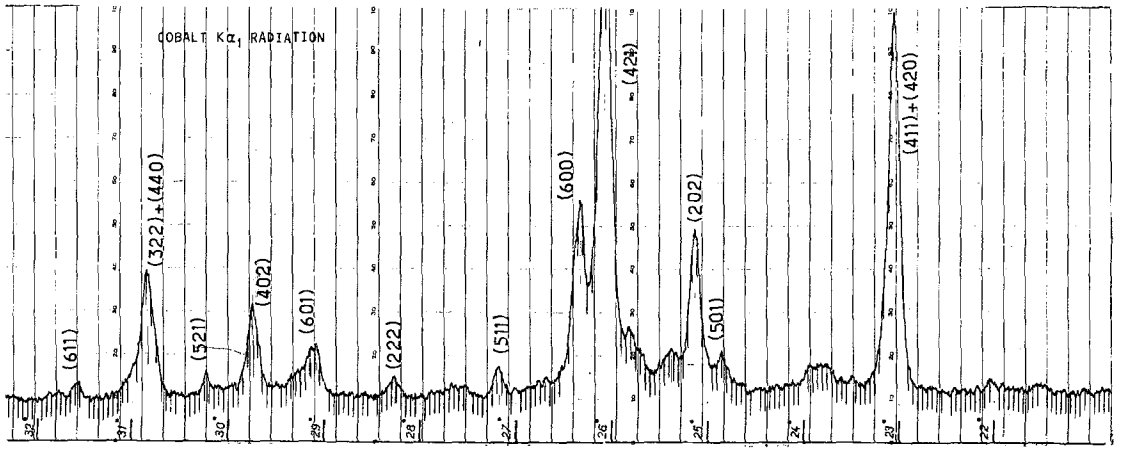

Figure 2 X-ray diffraction chart of extracted carbides. Some weak intensity lines come from another carbide, the cementite Fe_3C, which is also extracted during the anodic dissolution process.

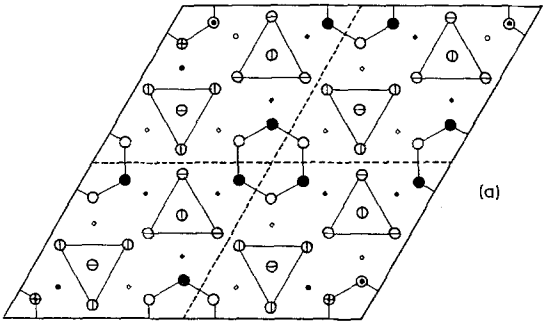

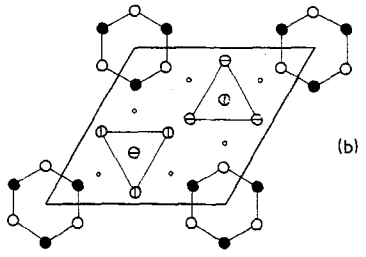

(c)

		Cr_7C_3 (a) WESTGREN'S DESCRIPTION	(b) Ru_7B_3	Cr_7C_3 SYMMETRICAL UNIT CELL
CHROMIUM OR RUTHENIUM ATOMS	○	0	0	0
	●	0.5	0.5	0.5
	⊙	0		0.8765
	⊕	0.5		0.3765
	⊖	0.25	0.318	0.1882
	◐	0.75	0.813	0.6882
CARBON OR BORON ATOMS	○	0.5	0.58	0.454
	•	0		0.954
	◇	0.5		0.421
	◆	0	0.08	0.921

Figure 3 Crystallographic structures of Cr_7C_3 and Ru_7B_3. (a) Unit cell of Cr_7C_3 as given by Westgren [1]. The projection of the atoms onto the basal plane is composed of four equal parts. (b) Unit cell of Ru_7B_3 as given by Aronsson [15]. (c) z co-ordinates of the chromium, ruthenium, carbon and boron atoms in Cr_7C_3 and Ru_7B_3. The third column gives the z co-ordinates of the atoms in a "perfectly symmetrical" unit cell of Cr_7C_3. Some values differ slightly from those proposed by Westgren.

TABLE II Atomic positions of chromium and carbon in Cr_7C_3: (a) values given by Westgren [1], (b) values obtained from a "perfectly symmetrical" unit cell

Atomic positions	(a) Cr_7C_3 Westgren's unit cell			(b) Cr_7C_3 "Perfectly symmetrical" unit cell		
	x	y	z	x	y	z
Chromium atoms						
6 c 1	0.06	0.12	0	0.0633	0.1266	0.8765
6 c 1	0.44	0.06	0	0.4366	0.0633	0
6 c 1	0.56	0.12	0.5	0.5633	0.1266	0.5
6 c 1	0.62	0.06	0	0.6266	0.0633	0
6 c 1	0.27	0.04	0.75	0.2700	0.0400	0.6882
6 c 1	0.27	0.23	0.75	0.2700	0.2300	0.6882
6 c 1	0.46	0.23	0.75	0.4600	0.2300	0.6882
6 c 1	0.54	0.27	0.25	0.5400	0.2700	0.1882
6 c 1	0.33	0.16	0.25	0.3333	0.1666	0.1882
2 b 3	0.33	0.66	0.25	0.3333	0.6666	0.1882
Carbon atoms						
6 c 1	0.20	0.10	0	0.1885	0.0942	0.9548
6 c 1	0.40	0.10	0.5	0.4057	0.0942	0.4217
6 c 1	0.40	0.30	0.5	0.4057	0.3115	0.4217
6 c 1	0.60	0.20	0	0.5942	0.1885	0.9217

Co-ordinates of equivalent positions:
6 c 1: $x\,y\,z; \bar{y}, x-y, z; y-x, \bar{x}, z; y, x, 1/2+z; \bar{x}, y-x, 1/2+z; x-y, \bar{y}, 1/2+z$
2 b 3: $1/3, 2/3, z; 2/3, 1/3, 1/2+z$

Cr_7C_3 as a superstructure with four times the volume of Ru_7B_3 (Fig. 4b). The carbides Mn_7C_3, Fe_7C_3 as well as the high-temperature form of Cr_7C_3 given by Rouault *et al.* can also be linked to Ru_7B_3. These structures which have orthorhombic cells and a ratio b/a close to the characteristic value $\sqrt{3}$, can also be considered as superstructures of Ru_7B_3 but this time with double the volume (Fig. 4c).

In all of these cells, the metal atoms are placed at the corners of octahedrons, tetrahedrons, acute-angled prisms and prisms which are almost right-angled (Fig. 5). The boron or carbon atoms are situated at the centre of each right-angled prism. These solid figures are more or less distorted. They are particularly so in Westgren's approximate description, less so in that of Rouault's and hardly at all in Ru_7B_3 (Table III). In the latter structure,

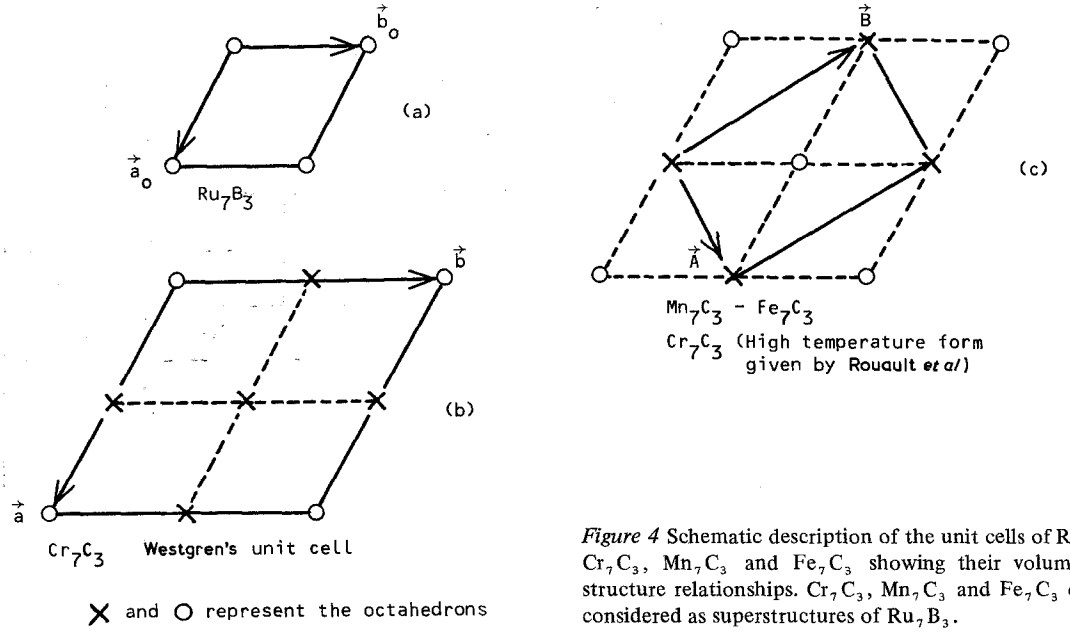

Figure 4 Schematic description of the unit cells of Ru_7B_3, Cr_7C_3, Mn_7C_3 and Fe_7C_3 showing their volume and structure relationships. Cr_7C_3, Mn_7C_3 and Fe_7C_3 can be considered as superstructures of Ru_7B_3.

TABLE III Values of distances and angles between atoms in: (a) Cr_7C_3 "perfectly symmetrical" unit cell, (b) Cr_7C_3 Westgren's unit cell [1], (c) Ru_7B_3, (d) Cr_7C_3 Rouault *et al.*s unit cell [2]

	(a) "Perfectly symmetrical" unit cell	(b) Westgren's unit cell	(c) Ru_7B_3	(d) Rouault *et al.*s unit cell
Distances				
a–b	2.6454	2.5164	2.7307	2.6050
a–c	2.7177	2.6917	2.8352	2.7043
a–e	2.6454	2.5164	2.7307	2.6050
f–b	2.7178	2.6917	2.8352	2.6997
f–c	2.6454	2.5164	2.7307	2.6050
f–d	2.6454	2.5164	2.7307	2.6050
f–e	2.7177	2.6917	2.8352	2.7043
b–e	2.6454	2.5164	2.7307	2.6050
e–d	2.7177	2.6917	2.8352	2.7101
d–c	2.6454	2.5164	2.7307	2.6050
c–b	2.7177	2.6917	2.8352	2.6997
g–h	2.7177	2.7361	2.8429	2.7402
g–j	2.7178	2.7362	2.8429	2.7419
g–i	2.7178	2.7362	2.8429	2.7402
h–j	2.6454	2.6562	2.7546	2.5861
j–i	2.6454	2.6562	2.7546	2.5862
i–h	2.6454	2.6562	2.7546	2.5840
m–l	2.6318	2.8204	2.8659	2.6705
n–q	2.6317	2.7844	2.8593	2.6929
o–p	2.6317	2.7844	2.8593	2.6909
n–m	2.7178	2.6917	2.8352	2.7043
m–o	2.7177	2.6917	2.8352	2.7102
o–n	2.6454	2.5164	2.7307	2.6050
q–l	2.7177	2.7361	2.8429	2.7419
l–p	2.7178	2.7362	2.8429	2.7402
p–q	2.6454	2.6562	2.7546	2.5861
c–m	2.0375	2.4643	2.1511	2.0112
c–n	2.0374	2.1109	2.1596	2.0256
c–o	2.0373	2.1109	2.1596	2.0305
c–l	2.0375	1.9722	2.2000	2.0730
c–p	2.0375	1.9406	2.1508	2.0808
c–q	2.0375	1.9406	2.1508	2.0793
r–v	2.6318	2.8204	2.8659	2.6704
s–w	2.6317	2.7844	2.8593	2.6909
t–u	2.6317	2.7844	2.8593	2.6929
s–r	2.7177	2.6917	2.8352	2.7102
r–t	2.7178	2.6917	2.8352	2.7043
t–s	2.6454	2.5164	2.7307	2.6050
w–v	2.7178	2.7362	2.8429	2.7402
v–u	2.7177	2.7361	2.8429	2.7419
u–w	2.6454	2.6562	2.7546	2.5861
Angles (°)				
om–ml	90.00	84.78	90.94	89.43
ml–lp	90.00	94.36	88.92	90.14
lp–po	90.00	84.64	90.92	100.58
po–om	90.00	96.19	89.21	79.74
tr–rv	122.15	125.82	120.94	121.32
rv–vu	57.85	53.89	59.00	58.74
vu–ut	122.15	125.50	120.90	122.06
ut–tr	57.85	54.75	59.17	57.90

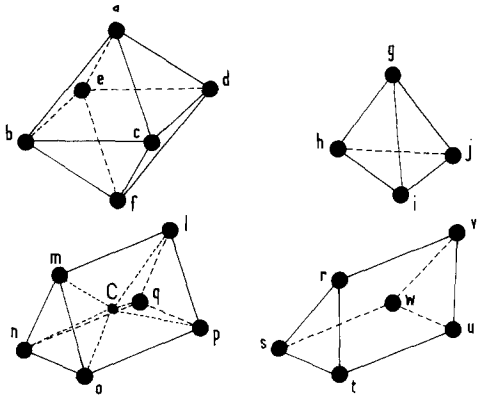

Figure 5 Solid figures obtained by joining metal atoms in Cr_7C_3 and Ru_7B_3.

the prisms which contain the boron atoms are right-angled, the boron atoms are placed at the centre of gravity and all the interatomic distances between metal and boron atoms are identical. This type of "perfectly symmetrical" environment is also observed in some other structures, for example in Fe_3C, Cr_3C_2, Pd_3B, Pd_3P, Pd_3Si, V_3B_2 and Re_3B [16].

By analogy with Ru_7B_3 and with these latter structures, one can postulate that the prisms contained in Cr_7C_3 are also "perfectly symmetrical. The approximate co-ordinates of the chromium and carbon atoms given by Westgren are modified in order to obtain this result. The hypothesis seems valid since the values obtained in this way) shown in Table IIb) give a better agreement between the calculated and the experimental diffracted intensities than those deduced from the other crystallographic descriptions of Cr_7C_3 (Table IV). Further experiments are currently being undertaken on single crystals to validate this hypothesis and to obtain more accurate values for the x, y and z co-ordinates for the chromium and carbon atoms.

TABLE IV Comparison between experimental (I_{exp}) and calculated (I_{cal}) diffraction intensities

($h\,k\,l$)	I_{exp}	(a) Cr_7C_3 Westgren's description		(b) Cr_7C_3 Rouault *et al.*s description		(c) Cr_7C_3 "perfectly symmetrical" unit cell	
		I_{cal}	$\lvert I_{cal}-I_{exp}\rvert$	I_{cal}	$\lvert I_{cal}-I_{exp}\rvert$	I_{cal}	$\lvert I_{cal}-I_{exp}\rvert$
(4 0 0) + (3 0 1)	9	15.9	6.9	4.1	4.8	12.6	3.6
(4 2 0) + (4 1 1)	100	100		100		100	
(2 0 2)	90	121.0	31.0	56.1	33.8	92.9	2.9
(5 0 1)	18	20.6	2.6	0	18	18.3	0.3
(4 2 1)	204	141.7	62.2	118.2	85.7	220.4	16.4
(6 0 0)	24	22.9	1.0	12.3	11.6	22.5	1.4
(2 2 2)	7	7.1	0.1	4.9	2.0	9.3	2.3
(6 0 1)	30	57.9	27.9	12.7	17.3	30.4	0.4
(4 0 2)	38	58.5	20.5	28.6	9.3	58.4	20.4
(5 2 1)	8	10.0	2.0	0	8.0	7.8	0.1
(3 2 2) + (4 4 0)	49	28.0	20.9	18.4	30.5	45.7	3.2
(8 0 1)	6	8.7	2.6	6.2	0.2	7.9	1.9
(4 0 3)	13	2.8	10.1	10.5	2.4	20.5	7.5
(1 0 0 0)	7	7.1	0.1	4.7	2.2	9.0	2.0
(6 0 3)	35	15.0	19.9	25.0	9.9	43.0	8.0
(6 4 2)	40	52.1	12.1	25.3	14.6	47.3	7.3

I_{exp}, intensities of some diffraction lines measured on X-ray diffraction charts of extracted carbides. The patterns were made at the liquid nitrogen temperature so as to minimize the effects of thermal vibration on the intensities of the diffracted beams. Only the intensities of the lines for which there is no possibility of a super-imposition with a line of cementite have been reported. The pair (4 2 0) + (4 1 1) is taken as an intensity reference (the sum of their intensities has the value 100).

I_{calc}, calculated intensities for: (a) Cr_7C_3 Westgren's unit cell, (b) Cr_7C_3 Rouault *et al.*s unit cell, (c) Cr_7C_3 "perfectly symmetrical" unit cell. These theoretical intensities come from the following ratio [17]:

$$\frac{I_{h_1 k_1 l_1}}{I_{h_0 k_0 l_0}} = \frac{1+\cos^2\theta_m \cdot \cos^2 2\theta_1 \cdot \sin^2\theta_0 \cdot \cos\theta_0 \cdot n_1 F_1^2 D(\theta_1) \cdot H(\theta_1)}{1+\cos^2\theta_m \cdot \cos^2 2\theta_0 \cdot \sin^2\theta_1 \cdot \cos\theta_1 \cdot n_0 F_0^2 D(\theta_0) \cdot H(\theta_0)}$$

The atomic scattering factors of the "International Tables for X-ray Crystallography" [18] were used and the Debye $D(\theta)$ and Huang $H(\theta)$ factors were not taken into account. The calculations are absolutely valid at the temperature of 0 K.

$\lvert I_{cal}-I_{exp}\rvert$, absolute values of the difference between calculated and measured intensities of the lines. The best agreement is obtained for the "perfectly symmetrical" unit cell.

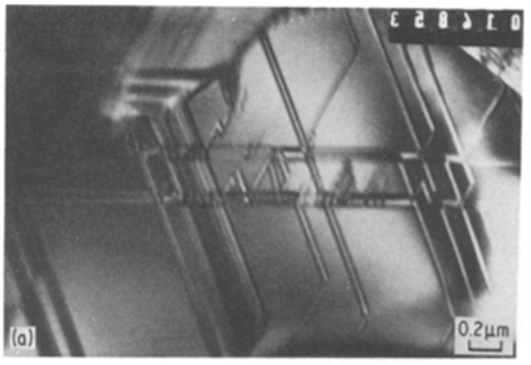

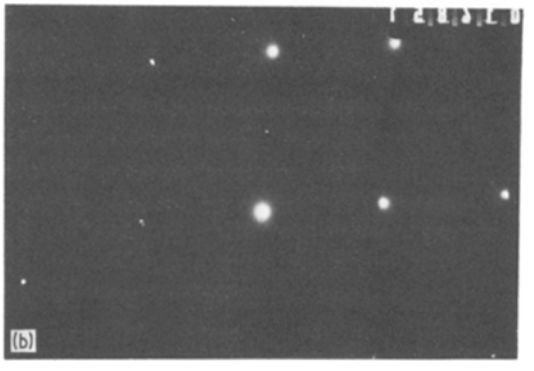

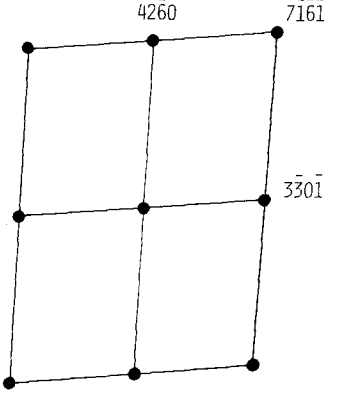

Figure 6 (a) Electron micrograph of a carbide showing three families of faults and a sub-grain boundary. (b) Corresponding electron diffraction pattern.

3.2. The stacking faults

The electron micrograph of Fig. 6a shows clearly the presence of numerous planar defects in the carbides. These are stacking faults which appear as linear black and white fringes. A maximum of three families of fringes with distinct orientations can be simultaneously observed in one crystal. Certain carbides seem to have more than three orientations but closer examination shows that they are, in fact, divided by sub-grain boundaries into a few monocrystalline zones of slightly different orientations. Inside each of these zones, only three orientations are to be found. Each of the three systems of fringes are observed equally frequently and have the same appearance.

A complete description of stacking faults requires knowledge of: (i) the fault plane $(h\,k\,i\,l)$, (ii) the fault vector **R**.

3.2.1. Determination of the stacking fault plane $(h\,k\,i\,l)$

The fault plane was determined by trace analysis and examination of the modifications caused in the electron diffraction patterns by the stacking faults.

3.2.1.1. Trace analysis. A large number of faults were examined and their traces drawn on the corresponding stereographic projections. In every case, it was found that the fault planes are lattice planes of the type $\{1\,\bar{1}\,0\,0\}$. No other type of fault planes has been observed. As an example, the trace analysis taken from the electron micrograph and the diffraction pattern given in Figs. 6a and b are shown in Fig. 7.

3.2.1.2. Modifications of the diffraction patterns due to the stacking faults. The electron diffraction patterns of the carbides which contain stacking faults show, for some particular orientations, diffraction streaks sometimes so elongated that they form continuous lines (Fig. 8). These lines

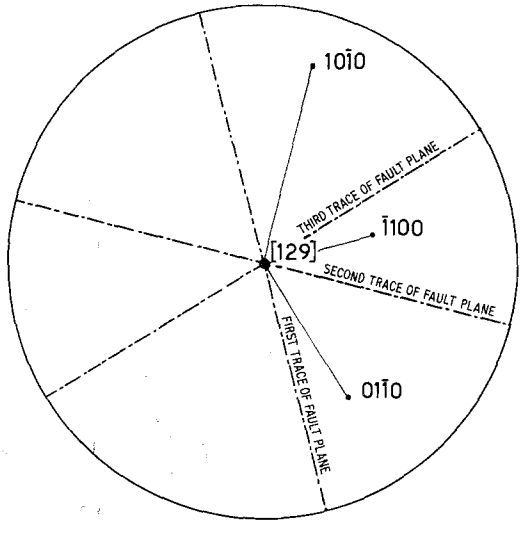

Figure 7 Trace analysis taken from the electron micrograph and the diffraction pattern of Fig. 6a and b. The traces of the fault planes correspond to the three equivalent lattice planes $(1\,0\,\bar{1}\,0)$, $(\bar{1}\,1\,0\,0)$ and $(0\,1\,\bar{1}\,0)$.

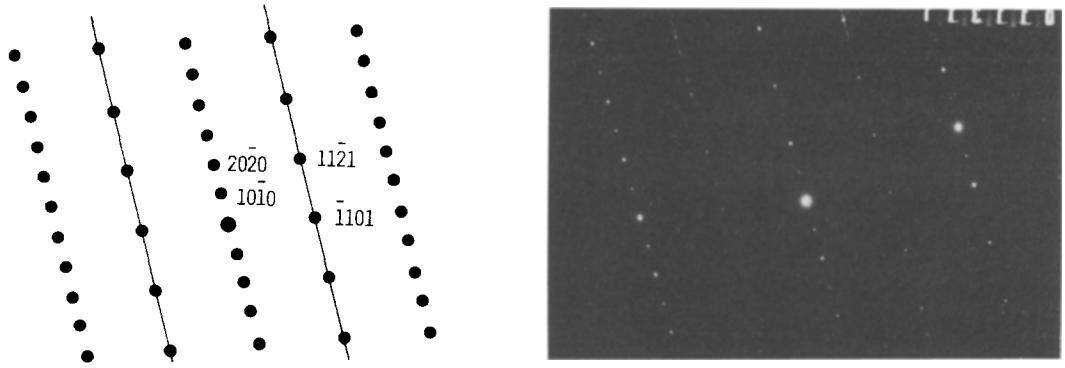

Figure 8 Electron diffraction pattern showing very elongated streaks along the reciprocal directions $1\,0\,\bar{1}\,0$. Notice that the streaks do not cross the spots with indice k even and are made up of a great number of tiny dots.

do not cross all the reciprocal lattice nodes. More particularly, they never cross the origin except where double diffraction occurs.

The streaks result from a planar disorder. A carbide crystal containing numerous stacking faults with fault planes $(h\,k\,i\,l)$ may be considered as being composed of a disordered stacking of planes $(h\,k\,i\,l)$. The loss of periodicity along the perpendicular to the planes generates, in the reciprocal lattice, streaks which are perpendicular to the fault planes.

All the streaks observed on diffraction patterns are oriented along the reciprocal directions of type $1\,\bar{1}\,0\,0$. This means that the fault planes are of the type $\{1\,0\,\bar{1}\,0\}$ and confirm the results previously obtained by trace analysis.

Streaks are also responsible for the presence of the additional spots which are sometimes observed on some diffraction patterns. The thinness of the foil creates an elongation of all the reciprocal lattice nodes over and above the effect due to the stacking faults. In the majority of cases, the streak and the elongation crossing the same node have different orientations and can, depending on the orientations of the foil and the faults, cut the Ewald's sphere at two points leading to the formation of two distinct reflections (Fig. 9). This effect is illustrated on the diffraction pattern given in Fig. 10.

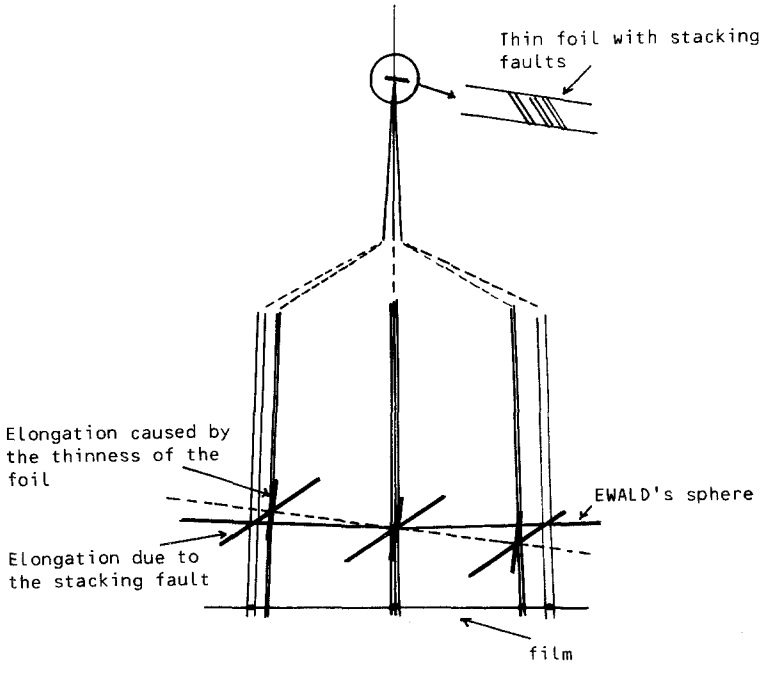

Figure 9 The figure shows how the Ewald's sphere can be cut at two points when the nodes of the reciprocal lattice undergo two distinct elongations. This effect gives extra reflections (see Fig. 10).

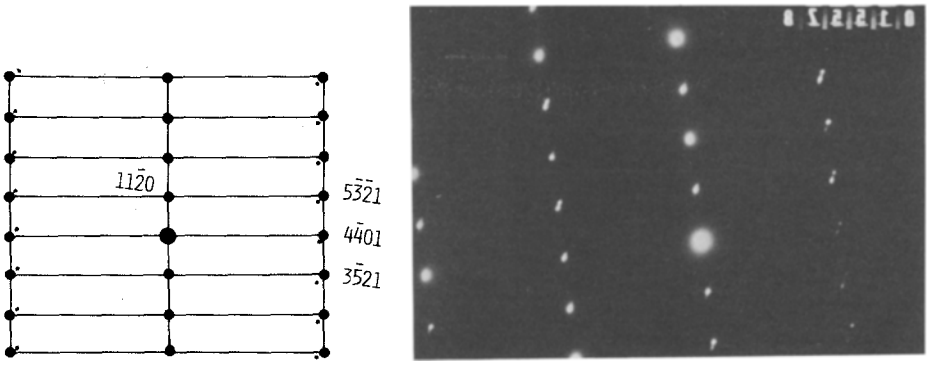

Figure 10 Electron diffraction pattern showing extra reflections caused by the thinness of the thin foil and the presence of stacking faults.

3.2.2. Determination of the fault vector **R**

The two-beam kinematic theory shows that the waves emitted by the two parts of a crystal situated on each side of a stacking fault suffer a phase difference $\alpha = 2\pi \mathbf{g}_{hkil} \cdot \mathbf{R}$. For some special diffracted beams $\mathbf{g}_{hkil}$, α can take the value $2k\pi$ and then all the waves emitted are in phase. Two important results follow.

(i) The first concerns the general nature of stacking fault contrast. The fault is invisible on electron micrographs (there is no contrast) when its image is formed with one of these special diffracted beams. For other vectors $\mathbf{g}_{hkil}$, the stacking fault appears as a system of black and white fringes.

(ii) The second consequence is related to the reciprocal lattice. All the nodes corresponding to these "in phase" vectors $\mathbf{g}_{hkil}$ are not affected by the fault. Therefore, they are not crossed by any streaks. These two results were used to determine the nature of the fault vector **R**.

3.2.2.1. Examination of stacking fault contrast. A large number of contrast experiments were conducted using many diffracted beams. The examinations were always coupled with trace analysis which allowed the fault plane indices $(h\,k\,i\,l)$ of the stacking fault to be defined. From all our experiments, it was found that the stacking faults with fault plane $(0\,1\,\bar{1}\,0)$, $(1\,0\,\bar{1}\,0)$ and $(1\,\bar{1}\,0\,0)$ are not in contrast when the vector $\mathbf{g}_{hkil}$ has respectively the indices h, k and $h + k$ even, whatever the values of the other indices may be. An example is given in Fig. 11.

3.2.2.2. Examination of streaks. The same conditions are found from the non-appearance of the streaks on electron diffraction patterns. The example given in Fig. 8 is related to a fault plane $(1\,0\,\bar{1}\,0)$. It shows that streaks pass through all the nodes apart those having the indices k even. So, the shortest translations **R** which agree with the results of these two kinds of observations are:

$$\mathbf{R}_{(0\,1\,\bar{1}\,0)} = \mathbf{a}/2$$

$$\mathbf{R}_{(1\,0\,\bar{1}\,0)} = \mathbf{b}/2$$

$$\mathbf{R}_{(1\,\bar{1}\,0\,0)} = (\mathbf{a} + \mathbf{b})/2$$

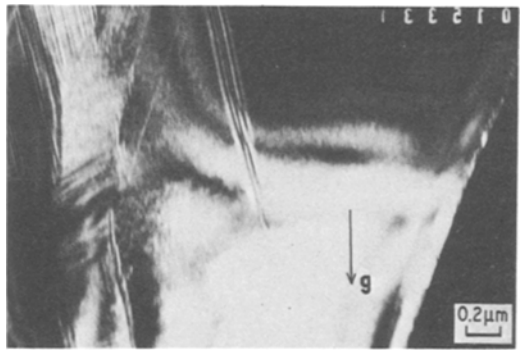

Figure 11 Dark-field image of a stacking fault using a $(4\,0\,\bar{4}\,2)$ reflection. No contrast is observed in the part of the crystal which follows the Bragg orientation.

3.2.2.3. Examination of the Laüe zone [0 0 0 1]. The [0 0 0 1] Laüe zone pattern shown in Fig. 12 is of particular interest as it confirms the previous results. This diffraction pattern contains no streaks although it exhibits the three streak directions $1\,0\,\bar{1}\,0$, $1\,\bar{1}\,0\,0$ and $0\,1\,\bar{1}\,0$ and all the dark field images obtained with any of its reflections do not produce any stacking fault contrast. Neither are the bright-field images contrasted; no contrast and

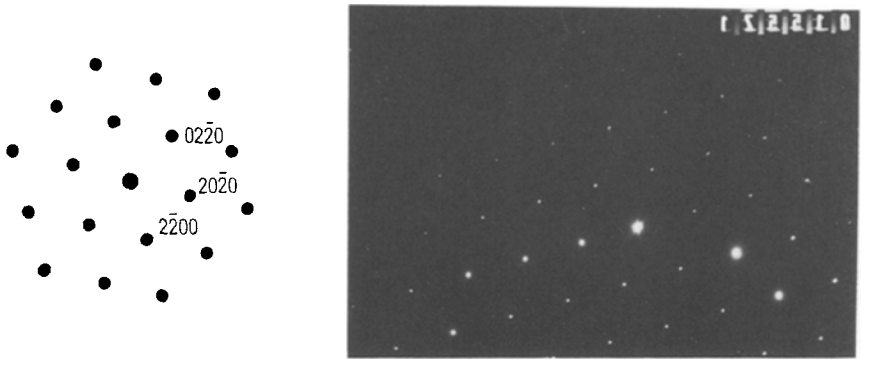

Figure 12 Electron diffraction pattern with [0 0 0 1] Laüe zone. No streaks are observed although their directions $1\,\bar{1}\,0\,0$, $0\,1\,\bar{1}\,0$ and $1\,0\,\bar{1}\,0$ are contained in the pattern.

no streaks are observed because all the reflections in the pattern have the indices h, k and $h + k$ simultaneously even. They all verify, therefore, without exception, the common conditions necessary for zero-contrast of stacking faults in the images and the absence of streaks on the diffraction patterns; double diffraction, even where it occurs, cannot produce a parasitic contrast.

4. Discussion

The stacking faults occur on the three equivalent lattice planes $(1\,0\,\bar{1}\,0)$, $(1\,\bar{1}\,0\,0)$ and $(0\,1\,\bar{1}\,0)$ and for each of these planes, only one single vector **R** located in the fault plane is to be found. Usually, the three fault planes exist simultaneously in the one crystal and they intersect in many places.

The effects of the formation of a stacking fault on the structure of M_7C_3 can be described in the following way. Let us consider, for example, the case of the stacking faults with fault plane $(1\,0\,\bar{1}\,0)$ and associated fault vector $\mathbf{R} = \mathbf{b}/2$. The structure of the carbide can then be regarded as composed exclusively of the right-angled prisms containing the carbon atoms we have previously spoken about (Fig. 13). These prisms, which are divided up into: (i) 3 x 2 continuous zig-zag rows

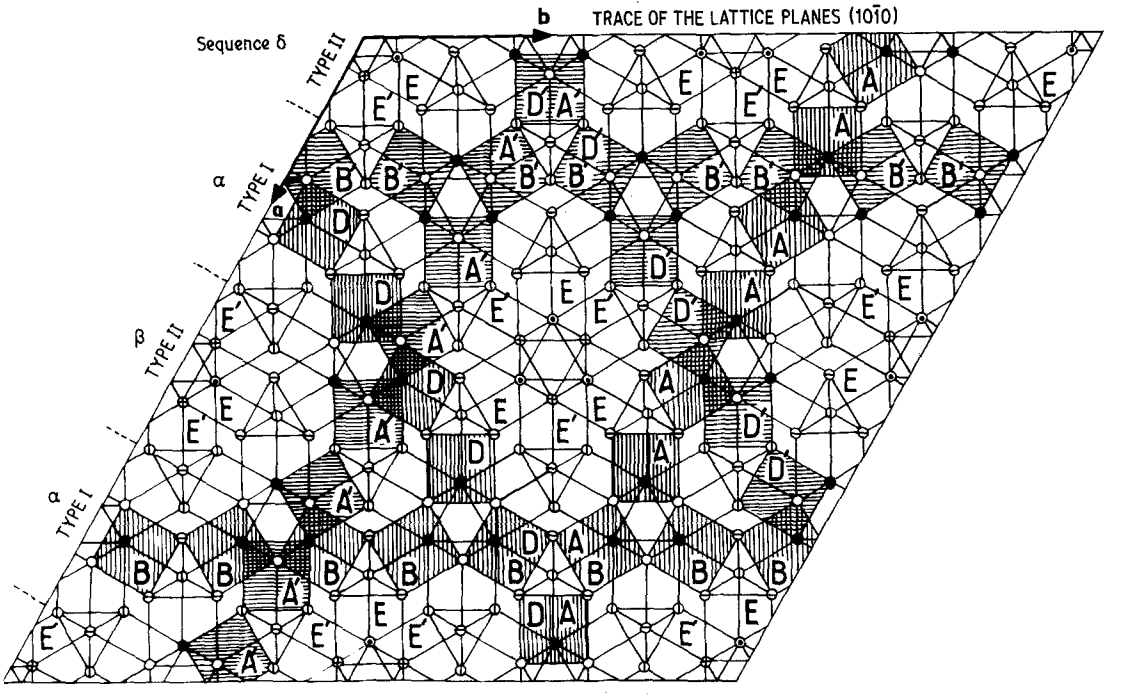

Figure 13 Description of the structure of Cr_7C_3 with the aid of six zig-zag rows (called AA′, BB′ and DD′) and isolated right-angled prisms (called E and E′). Only the prisms belonging to one of each row parallel to the three axes **a**, **b** and **d** are shaded. The prisms can be grouped, parallel to the lattice planes $(1\,0\,\bar{1}\,0)$ into the two types I and II (shown in Fig. 14) with the stacking sequence $\alpha\beta\alpha\delta\alpha\beta\alpha\delta$ . . . .

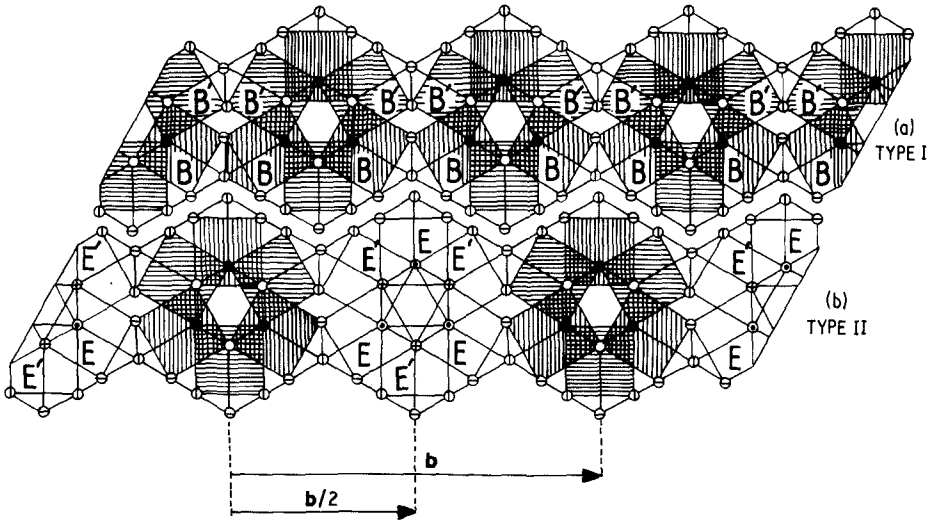

Figure 14 Description of layers of prisms grouped parallel to the axis **b** in: (a) type I, (b) Type II. Notice that a translation b/2: (i) does not modify the atomic positions in type I, (ii) modifies some of the atomic positions in type II. Types I and II can, respectively, be shown schematically with XXX and XOX.

called A,A′; B,B′ and D,D′ respectively parallel to the three axes **a**, **b** and **d** (ii) two isolated groups which do not form continuous rows, called E and E′, can be grouped, parallel to the $(1\,0\,\bar{1}\,0)$ planes into the two types I and II shown in Fig. 14.

Types I contain the prisms belonging to the continuous rows B and B′ parallel to the axis **b**. Their principal characteristic is that all their atoms without exception have a repeat distance with a translation **b**/2. Types II contain isolated prisms of the rows A,A′; B,B′; D,D′ and E,E′, and a translation **b**/2 in this case modifies the z co-ordinates of some atoms.

The perfect crystal is then easily described with the aid of this model. It is composed of a stacking of types I and II arranged in the sequence $\alpha\,\beta\,\alpha\,\delta\,\alpha\,\beta\,\alpha\,\delta\,\ldots$ (Figs. 13 and 16a). A stacking fault with a fault plane $(1\,0\,\bar{1}\,0)$ and a vector $\mathbf{R} = \mathbf{b}/2$ is created each time a part of the crystal is translated by a vector **b**/2. These translations would occur at the points in the crystal where the expenditure of energy is smallest. For that reason, they are probably located in the types I. We have previously indicated that in these types, the translations do not modify the co-ordinates of any of the atoms.

The stacking faults are often very numerous inside a single crystal of carbide and all those belonging to the one family are not always distributed randomly in the planes which act as their fault planes. Detailed observations of the streaks indicated some ordering. Usually, the streaks do not have a constant intensity but are often made up of a very large number of tiny dots (Fig. 8). Sometimes, strong intensity modulations which can be considered as true diffraction spots appear and replace the streaks (Fig. 15). These additional spots are always situated at definite positions between the normal spots and can never be indexed using the hexagonal unit cell. They are extra reflections caused by stacking faults which are arranged in an ordered manner. These experimental observations can be easily interpreted if one takes into account the two following extreme cases:

(i) Stacking faults are completely disordered. Stacking faults occur randomly in the types I. They produce, in the reciprocal lattice, streaks having a constant intensity along all their length. Stacking faults will appear in strong contrast each time their dark-field image is formed with any of the reflections containing streaks.

(ii) Stacking faults are perfectly ordered. A fault occurs every n type I. Consider, for example, the particular case for which $n = 1$. There is a fault in each of the types I.

Such an arrangement can be expected in carbides which contain a very large number of faults because there must exist inside them, domains of greater or smaller size in which all the types I are faulted. Two of these domains separated by a portion of non-faulted crystal are drawn in Fig. 16c. The two ordered domains have

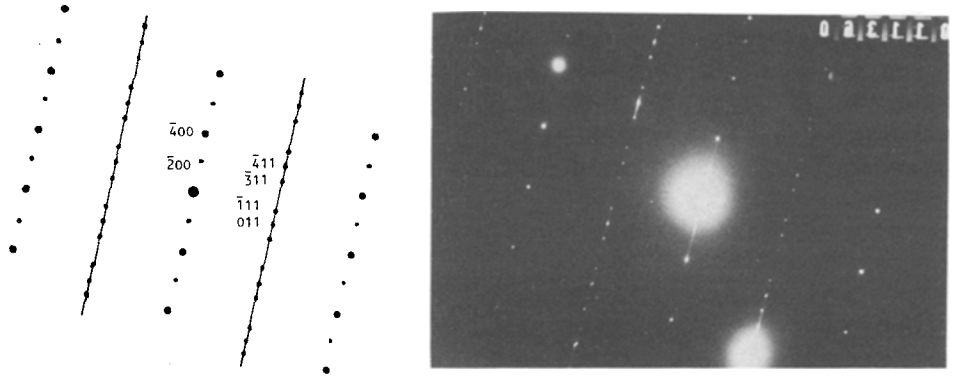

Figure 15 Electron diffraction pattern containing extra spots caused by ordered stacking faults. The pattern can be fully indexed with a monoclinic superlattice indicating that there is a fault in each type I ($n = 1$). The streak which crosses the origin is produced by the parasitic double diffraction phenomenon whose effect is very marked in the pattern.

a new stacking sequence of types I and II namely $\alpha\,\delta\,\alpha\,\delta\,\alpha\,\delta\,\ldots$, or $\alpha\,\beta\,\alpha\,\beta\,\alpha\,\beta$, and they form a superlattice which can be described using a monoclinic unit cell* (shown Fig. 16c) linked to the normal hexagonal unit cell by the following relationships:

$$\mathbf{A}_{\text{mono}} = 2\,\mathbf{a}_{\text{hex}}$$

$$\mathbf{B}_{\text{mono}} = \mathbf{b}_{\text{hex}}$$

$$\mathbf{C}_{\text{mono}} = \mathbf{c}_{\text{hex}}$$

The corresponding diffraction patterns are made up of "fundamental" and "superlattice" reflections. Fundamental dots are common to the hexagonal and monoclinic cells and they remain unmodified whether the crystal is faulted or not. Superlattice reflections only exist in the monoclinic cell and they are caused by the new periodicity introduced by the ordering of the faults. As they replace the streaks, they are compulsorily situated on their paths.

The diffraction pattern given in Fig. 15 can be fully indexed using this multiple monoclinic cell. The ordered domains can be small in size and then be separated by non-faulted domains, randomly faulted domains or faulted domains with variously ordered sequences. Fig. 16b gives the example of two faulted domains with a fault in each of the types I ($n = 1$) separated by a faulted domain with a fault every second types I ($n = 2$). As in ordered structures, an antiphase-boundary is created.

This argument can easily be extended to all other kinds of ordering. In a single carbide, various sequences of ordered stacking faults can simultaneously exist and each of these sequences produces extra spots. The addition of the different effects gives the streaks composed of the tiny dots discussed previously.

It must be remembered that only those spots located on the streak paths can produce contrast. When the ordered domains are very extensive, they give additional spots which are nearly sharp and hardly any contrast is observed. The stacking faults remain invisible. This result could be expected because the ordered domains can also be considered as having non-faulted superlattices. It has also been experimentally verified in view of the difficulty of observing any stacking fault contrast in very strongly faulted carbides. The number of faults in them is so great that the above configurations are to be found.

When the ordered domains are narrower, the extra spots become elongated and a contrast phenomenon appears at the boundaries of the different domains. Similarly, the antiphase boundaries, where they exist, will be contrasted.

The stacking faults observed in the carbides M_7C_3 can have several origins. They may result

*The superlattice can also be described using the orthorhombic unit cell drawn Fig. 16b. However, it is better to use a monoclinic cell because for every other value of n, the superlattices have monoclinic cells with axes:

$$\mathbf{A}_{\text{mono}} = N\,\mathbf{a}_{\text{hex}}$$

$$\mathbf{B}_{\text{mono}} = \mathbf{b}_{\text{hex}} \quad \text{(with } N \text{ integer)}$$

$$\mathbf{C}_{\text{mono}} = \mathbf{c}_{\text{hex}}.$$

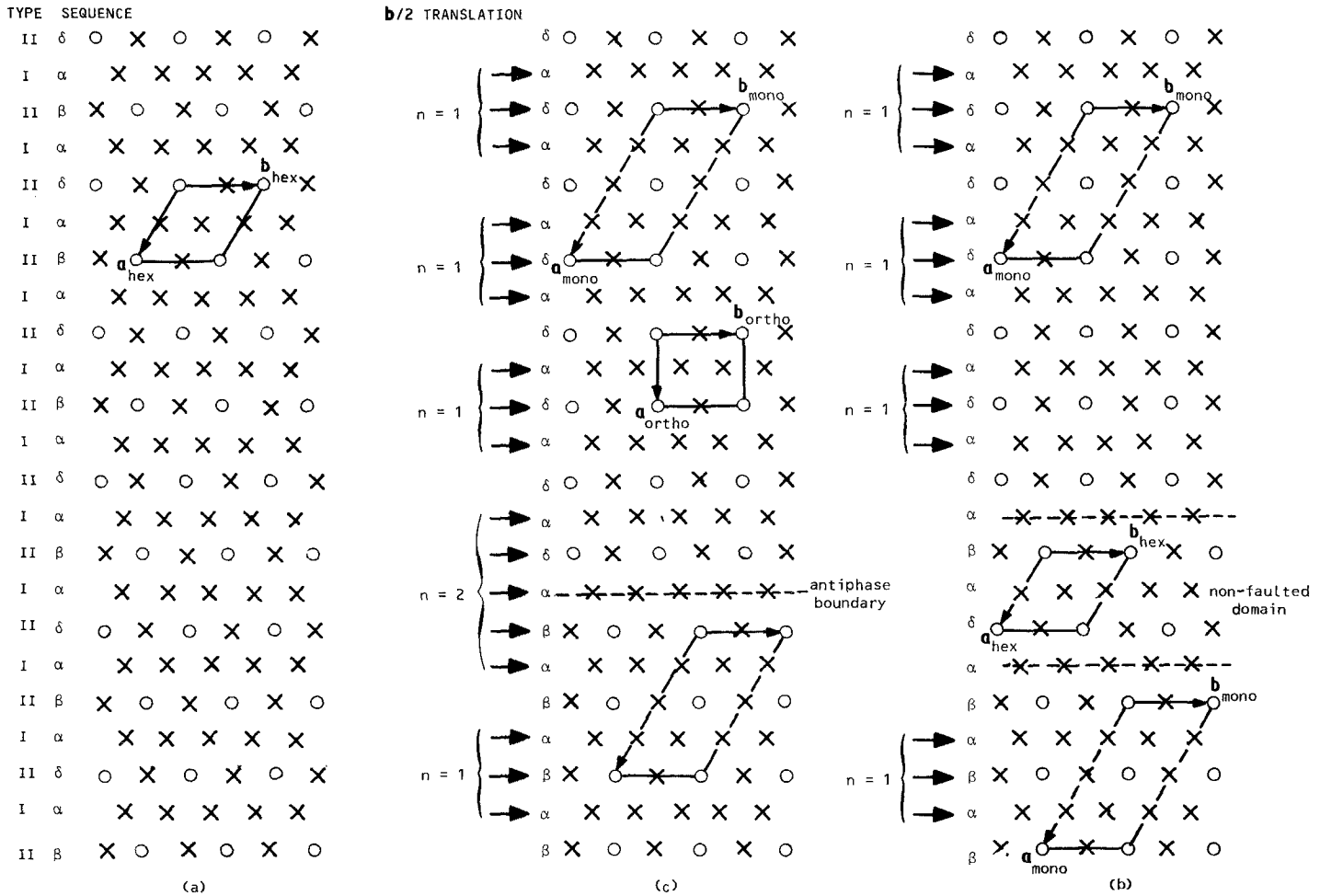

Figure 16 Schematic descriptions of the structure of non-faulted and faulted crystals of Cr_7C_3 by means of a stacking up of types I and II. (a) Non-faulted crystal. The stacking sequence is $\alpha\beta\alpha\delta\alpha\beta\alpha\delta$ . . . . (b) Faulted crystal. Two faulted domains with $n = 1$ are separated by a portion of non-faulted crystal. The stacking sequences of ordered domains are $\alpha\delta\alpha\delta\alpha\delta$ . . . or $\alpha\beta\alpha\beta\alpha\beta$ . . . . (c) Faulted crystal. Two domains with $n = 1$ are separated by a domain with $n = 2$. An antiphase boundary is created.

from thermal or mechanical stresses which act in the already formed crystal. The stresses produce a plastic deformation of the crystal by means of partial dislocations in the fault planes. However, no partial dislocations have ever been observed at the edges of a stacking fault. This may suggest that the stacking faults are directly formed in the liquid state during the nucleation and growth of the carbides. At the very beginning of the crystallization process, some nuclei may exist in the liquid and these may join together to form a single crystal containing stacking-faults and sub-grain boundaries.

5. Conclusions

The carbides found in white cast-iron samples (which had received no further treatment after solidification) contain about 35% chromium, 9% vanadium, 46% iron and 9% carbon and appear as needles in the shape of hexagonal prisms.

Electron microprobe analysis and X-ray diffraction studies show that they are $Cr_{2.8}V_{0.7}Fe_{3.4}C_3$ mixed carbides of the type M_7C_3. They are stoichiometric with respect to carbon and isomorphic with Cr_7C_3. The shape of the cell is perfectly hexagonal and corresponds to the chromium carbide unit cell earlier described by Westgren. It does not correspond to Rouault *et al.*s orthorhombic unit cell nor to the orthorhombic cell of Fe_7C_3. The content of the cell is imprecisely known, nonetheless Westgren's approximate description allows us to consider it as made up of layers of almost right-angled trigonal prisms, each of which contains a carbon atom located near its centre of gravity. A similar environment of carbon atoms, this time "perfectly symmetrical", has been reported to exist in Ru_7B_3 and in several other structures. So, by analogy with this, a structure composed of perfect right-angled prisms with a carbon atom situated at the centre of gravity is suggested for M_7C_3.

The results obtained in this way lead to a good agreement between the calculated and the diffracted intensities measured on X-ray diffraction patterns of extracted carbides. Further X-ray diffraction studies on a single crystal should verify this hypothesis.

Planar defects were studied simultaneously, by electron microscopy and electron diffraction. The techniques of image-contrast and trace-analysis were used in electron micrography and all the anomalies and modifications caused by the faults were studied on electron diffraction patterns.

The experimental results show that the fault planes are the three equivalent planes $(1\,0\,\bar{1}\,0)$, $(1\,\bar{1}\,0\,0)$ and $(0\,1\,\bar{1}\,0)$ and that for each of them there is a single fault vector contained in the plane, namely:

$$\mathbf{R}_{(0\,1\,\bar{1}\,0)} = \mathbf{a}/2$$

$$\mathbf{R}_{(1\,0\,\bar{1}\,0)} = \mathbf{b}/2$$

$$\mathbf{R}_{(1\,\bar{1}\,0\,0)} = (\mathbf{a}+\mathbf{b})/2.$$

A simple model is proposed which views the structure of M_7C_3 as a stacking sequence of right-angled prisms containing carbon atoms. This model suggests that the stacking fault energy is very weak. Their formation produces only slight structural changes because, in the hexagonal cell, most of the atoms have a repeat for the three translations $\mathbf{a}/2$, $\mathbf{b}/2$ and $(\mathbf{a}+\mathbf{b})/2$, equivalent to the three fault vectors **R**. This explains why stacking faults occur so frequently in the carbides.

When the fault density is great, all the faults belonging to one of the three families do not exist randomly in their fault planes but may have a definite order which has been deduced from the examination of anomalies on electron diffraction patterns. No other crystalline defects (partial dislocations for example) have been observed in the present samples.

References

1. A. WESTGREN, *Jernkont. Ann.* **119** (1935) 231.
2. A. ROUAULT, P. HERPIN and R. FRUCHART, *Ann. Chim.* **5** (1970) 461.
3. E. L. KOLOSOVA, V. I. SYREYSHCHIKOVA, M. I. GOL'DSHTEYN, L. B. LASHENKO and G. D. SUSLOPAROV, *Fiz. Metal. Metallowed.* **38** (1974) 436.
4. L. R. WOODYATT and G. KRAUSS, *Met. Trans. A* **7A** (1976) 983.
5. D. J. DYSON and K. W. ANDREWS, *J. Iron Steel Inst.* **207** (1969) 208.
6. K. KUO, *ibid* **179** (1953) 363.
7. J. BEECH and D. H. WARRINGTON, *ibid* **204** (1966) 460.
8. S. NAGAKURA and S. OKETANI, *Trans. ISIJ* **8** (1968) 265.
9. M. TANINO, *Bull Japan Inst. Metals* **11** (1972) 203.
10. P. B. HIRSCH, A. HOWIE, R. B. NICHOLSON, D. W. PASHLEY and M. J. WHELAN, "Electron Microscopy of thin Crystals" (Butterworths, London, 1965) p. 313.
11. R. GEVERS, J. VAN LANDUYT and S. AMELINCKX, *Phys. Stat. Sol.* **21** (1967) 393.
12. M. J. WHELAN and P. B. HIRSCH, *Phil. Mag.* **2** (1957) 1303.
13. R. BENZ, J. F. ELLIOT and J. CHIPMAN, *Met.*

Trans. 5 (1974) 2235.
14. J. P. BOUCHAUD, *Ann. Chim.* **2** (1967) 353.
15. B. ARONSSON, *Acta Chem. Scand.* **13** (1959) 109.
16. B. ARONSSON and S. RUNDQUIST, *Acta Cryst.* **15** (1962) 878.
17. C. FRANTZ, Thèse, Nancy (1970).
18. "International Tables for X-ray Crystallography", published for The International Union of Crystallography, Vol. IV (Kynoch Press, Birmingham, 1974).

Received 5 July and accepted 16 October 1979.